Supporting Information

Bithiophene-Linked Conjugated Polymers Featuring Intrinsic Active Sites for Efficient Solar-Driven Hydrogen Production

Yuchen Cong,[†a] Wanjun Tang,[†a] Pengyu Ma,[a] Jianye Zou,[a] Ying Zhang[*a]

a. School of Integrated Circuits, AnHui University, Hefei, Anhui 230601, China.

† These authors contributed equally to this work

**Correspondence to Y. Z. (yingz@ahu.edu.cn)*

Materials and Syntheses

All reagents and solvents were used as received from commercial suppliers unless otherwise noted. Trifluoromethanesulfonic acid (CF_3SO_3H, 98%), ferric chloride (anhydrous for synthesis), 2-thiophenecarbonitrile (99%) were purchased from Sigma-Aldrich. 1,3,5-tris-2-thienyl-benzene (>98%) was purchased from TCI. Sodium sulfate anhydrous (Na_2SO_4, 99.99% metals basis), sodium bicarbonate ($NaHCO_3$, ≥99.8%) were purchased from Aladdin BioChem Technology Co. Ltd. All organic solvents, including chloroform (≥99%), tetrahydrofuran (≥99%), and acetone (>99%) were purified prior to use. The water used in all experiments was de-ionized (DI).

Synthesis of 2,4,6-tri(2-thienyl)-1,3,5-triazine (TTT). In a typical synthesis, 2-thiophenecarbonitrile (5 mmol) was dissolved in 30 mL of chloroform. Then the reaction mixture was cooled to 0 °C. CF_3SO_3H (1 mL, 11.3 mmol) was added dropwise under argon atmosphere and the reaction proceeded at room temperature for 48 h. The reaction was stopped and the mixture was neutralized with aqueous $NaHCO_3$. The organic layer was washed with water and concentrated under reduced pressure. The product was purified by recrystallizing (1.4 g, 85%).^{1}H NMR (400 MHz, $CDCl_3$): δ (ppm) = 8.28 (d, 3H), 7.61 (d, 3H), 7.18 (d, 3H).

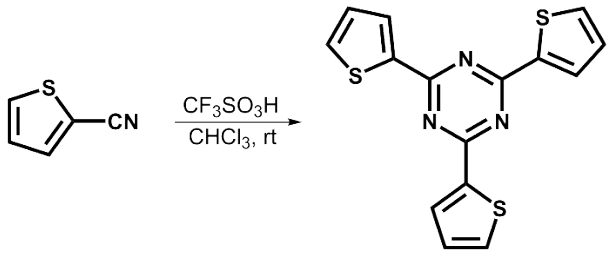

Supplementary Scheme 1. Synthetic procedure for TTT.

Synthesis of PTTT and PTTB: In a typical synthesis, 2,4,6-tri(2-thienyl)-1,3,5-triazine or 1,3,5-tris(2-thienyl)benzene (100 mg) was dissolved in 10 mL of chloroform. A solution

of ferric chloride (200 mg) in chloroform (20 mL) was added dropwise under an argon atmosphere, and the reaction mixture was stirred at room temperature for 48 h. After completion of the reaction, the resulting product was collected by filtration and successively washed with water, hydrochloric acid, and chloroform. The crude product was further purified by Soxhlet extraction with deionized water and tetrahydrofuran (THF), followed by drying under vacuum at 60 °C for 24 h to afford PTTT or PTTB.

General Characterizations

Fourier transform infrared (FTIR) spectra were recorded on a Thermo Nicolet 6700 spectrometer over the range of 4000–500 cm^{-1}. Powder X-ray diffraction (PXRD) patterns were collected using a Bruker D8 Advance diffractometer. Solid-state ^{13}C NMR spectra were acquired on a Bruker Avance III 600 MHz spectrometer. X-ray photoelectron spectroscopy (XPS) measurements were performed using a Thermo Scientific ESCALAB 250 spectrometer. High-resolution transmission electron microscopy (HRTEM) images were obtained on a JEOL JEM-2010 microscope operated at an accelerating voltage of 200 kV. Scanning electron microscopy (SEM) images were collected using a Hitachi SU8220 cold field-emission scanning electron microscope operated at 5 kV. Nitrogen physisorption measurements were carried out at 77 K on a Micromeritics TriStar 3020 surface area and pore analyzer. UV–vis diffuse reflectance spectra were recorded at room temperature using a Shimadzu DUV-3700 spectrophotometer, with $BaSO_4$ employed as a reflectance standard. Steady-state photoluminescence (PL) spectra were collected using a FluoroMax-4 spectrofluorometer (Horiba Scientific) and analyzed with FluoroEssence v2.2 software. Thermogravimetric analysis (TGA) was performed at a heating rate of

10 °C/min under N_2 (TA Instruments Q5000IR). Metal concentrations were determined using a Thermo Scientific PlasmaQuad 3 inductively coupled plasma (ICP) instrument.

Synchrotron Radiation Photoemission Spectroscopy (SRPES): SRPES experiments were performed at the Photoemission End station (BL10B) in the National Synchrotron Radiation Laboratory in Hefei, China. To obtain the secondary electron cutoff, an excitation of 168.80 eV was utilized. The binding energy (BE) was calibrated and referenced to the E_f of a gold foil. The work function (Φ) of samples was determined according to equation Φ = hv-ΔE, where is ΔE is the spectrum width, i.e. the energy difference between the secondary electron cutoff and the Fermi level of the tested sample. To obtain the secondary electron cutoff, a -10 V bias was applied to the sample, which accelerated all the photoelectrons with higher kinetic energy (KE) to overcome the WF of the analyzer.

***In situ* Near Edge X-ray Absorption Fine Structure (NXANES) Spectroscopy:** The measurements were performed at the photoemission end-station at beamline BL10B in the National Synchrotron Radiation Laboratory (NSRL) in Hefei, China. The beamline is connected to a bending magnet and covers photon energies from 100 to 1,000 eV with a resolving power (E/ΔE) better than 1,000. The end-station is composed of four chambers—an analysis chamber, a preparation chamber, a load-lock chamber, and a high-pressure reactor. The analysis chamber, with a base pressure of $< 2 \times 10^{-10}$ torr, is connected to the beamline with a VG Scienta R3000 electron energy analyzer and a twin anode X-ray source with an argon plasma treatment (300 W).

***In situ* diffuse reflectance infrared Fourier transform spectroscopy (*in situ* DRIFTS) measurements** were performed using a Bruker IFS 66v Fourier-transform spectrometer equipped with a Harrick diffuse reflectance accessory. Each spectrum

was recorded by averaging 256 scans at a 2 cm^{-1} spectral resolution. The samples were held in a custom-made IR reaction chamber which was specifically designed to examine highly scattering powder samples in the diffuse reflection mode. The chamber was sealed with two ZnSe windows.

Photocatalytic Water Splitting Experiments: In a typical experiment, 100 mg of catalyst was dispersed in 100 mL of water containing 0.01 M triethylamine as a sacrificial agent and sonicated for 30 min to ensure uniform dispersion. Dissolved air was removed by purging the reactor with argon for 30 min prior to irradiation. Visible-light irradiation (λ > 420 nm) was provided by a 300 W Xe lamp (Perfect Light PLS-SXE 300) equipped with a cutoff filter (Kenko L-42) at an average intensity of 100 $mW \cdot cm^{-2}$. Hydrogen evolution was quantified by gas chromatography (Shimadzu GC-2014) using a thermal conductivity detector (TCD) with argon as the carrier gas.

Photocurrent measurements: All electrochemical measurements were performed using a Metrohm Autolab PGSTAT302N potentiostat/galvanostat in a standard three-electrode configuration, with a Pt wire as the counter electrode and Ag/AgCl (saturated KCl) as the reference electrode. Visible-light irradiation (λ > 420 nm) was provided by a 300 W Xe lamp (Perfect Light PLS-SXE 300) equipped with a cutoff filter (Kenko L-42). The electrolyte was purged with argon for 30 min prior to measurements.

Computational details

First-principles calculations were performed based on ab initio density functional theory (DFT) using Vienna *AB initio* Simulation Package (VASP) code.[1] The projector augmented wave (PAW)-Perdew, Burke, and Ernzerhof (PBE) along with DFT-D_3 method was used for calculate the Gibbs energy change during hydrogen production

reactions. A well-converged plane-wave cutoff of 520 eV was employed. The atomic coordinates were allowed to relax until the forces on the ions were less than 2×10^{-2} eV $Å^{-1}$ and the electronic convergence was set to be 1×10^{-5} eV.[2] Photocatalytic H_2 evolution reactions (HER) of PTTT and PTTB were simulated with the model proposed by Nørskov et al.[3] For finite oligomers with emergent edge states were simulated at the PBE-D3BJ/6-31g* level as implemented in the Gaussian16 program, the distribution of holes and electrons in the first excited state were analysed by Multiwfn.[4]

The HER on the polymer involves two one-electron steps with each step consuming an electron.[5]

$$\text{Step1: } * + H^+ + e^- \rightarrow *H$$

$$\text{Step2: } *H + H^+ + e^- \rightarrow *H_2$$

where * denotes an active site on the polymer surface, and *H indicates a hydrogen atom adsorbed at that site.

Gibbs free energy calculations are conducted to determine the Gibbs free energy changes (ΔG) for each step of the reaction. The Gibbs free energy changes ΔG are obtained using the formula:

$$G(T) = E + H(T) - TS(T)$$

where the E denotes the self-consistent field energy for a given species and enthalpy $H(T)$ or $S(T)$ can be calculated, accounting for all relevant finite temperature effects, including vibration, rotation, and translation for gas-phase species. For adsorbed species, only the vibration contribution of the fixed polymer material is considered, as rotational and translational motions are restricted. All calculations are performed at

298.15 K, pH=7, and the external potential is taken into account.

The ΔG are obtained through the follows:

$$\Delta G_1 = G(*H) - G(*) - 1/2\ G(H_2) + \Delta pH - eU_{red}$$

$$\Delta G_2 = G(H_2) + G(*) - G(*H) - 1/2\ G(H_2) + \Delta pH - eU_{red}$$

where $G(H^+ + e^-)$ is replaced by $1/2\ G(H_2)$. For photocatalytic reactions, U_{red} represents the potential for the hydrogen evolution reaction (HER). Here, U_{red} is defined as the energy difference between the conduction band minimum (CBM) and the hydrogen reduction potential (H^+/H_2).

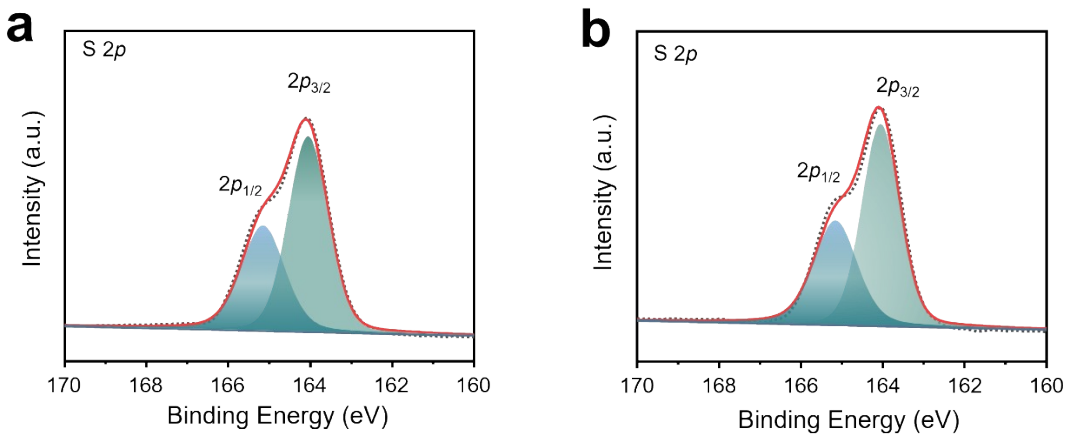

Fig. S1. High-resolution S 2*p* XPS spectra of (a) PTTT and (b) PTTB.

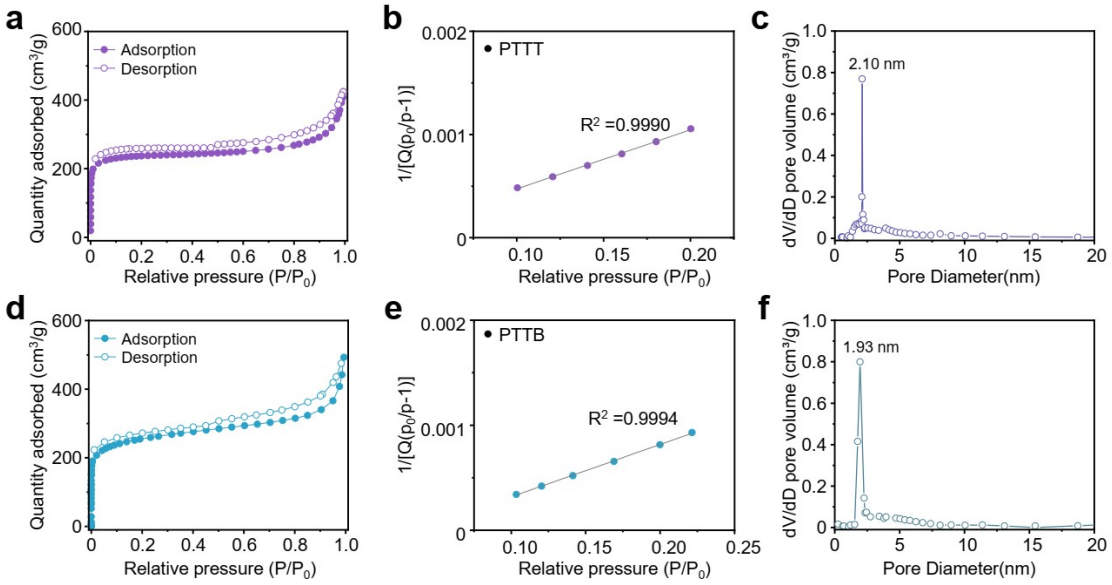

Fig. S2. N_2 adsorption–desorption isotherms of (a) PTTT and (d) PTTB; corresponding BET plots of (b) PTTT and (e) PTTB; and pore size distributions of (c) PTTT and (f) PTTB.

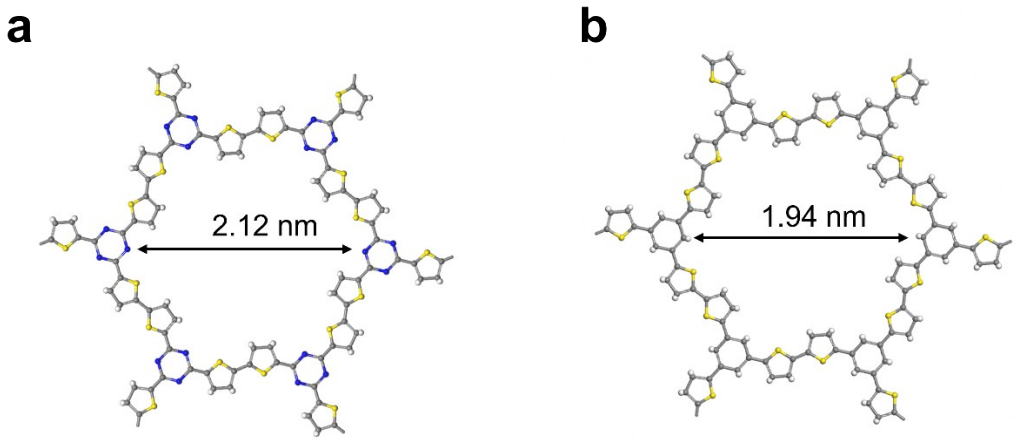

Fig. S3. Top view of (a) PTTT and (b) PTTB structures. Gray, white, blue, and yellow spheres represent C, H, N, and S atoms, respectively. The depicted structures are idealized models.

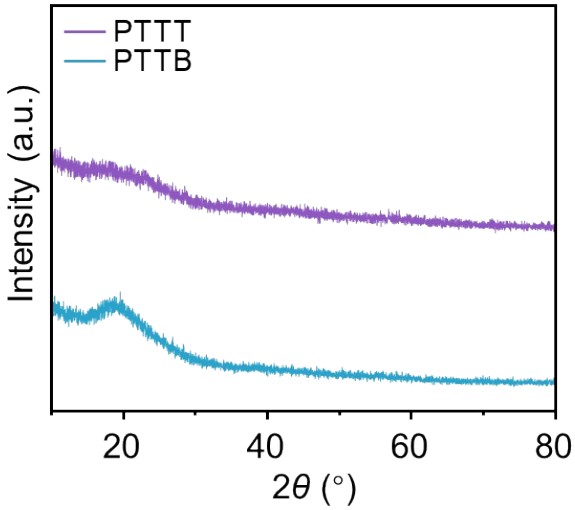

Fig. S4. PXRD patterns of PTTT and PTTB.

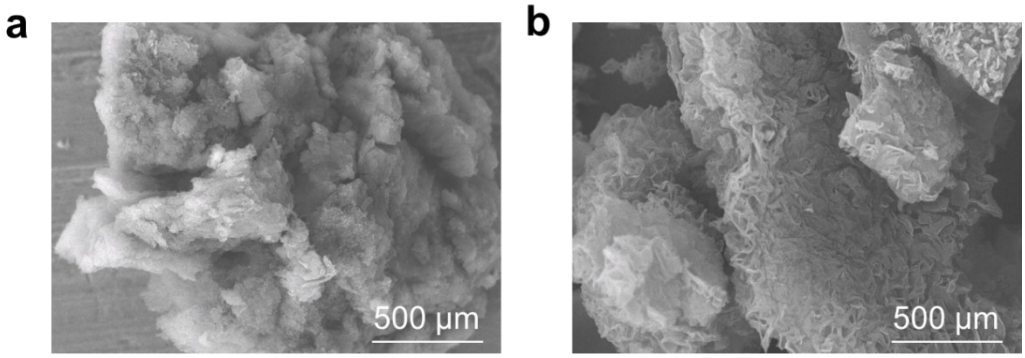

Fig. S5. SEM images of (a) PTTT and (b) PTTB.

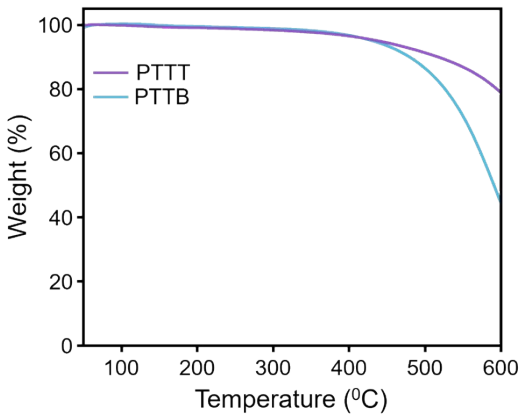

Fig. S6. Thermogravimetric analysis of PTTT and PTTB measured at a heating rate of 10 °C/min under N_2 atmosphere.

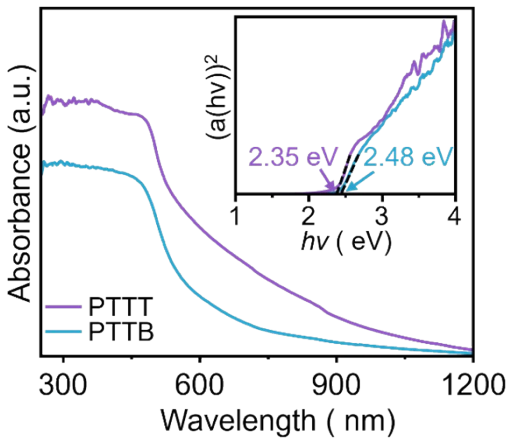

Fig. S7. UV-vis-NIR diffuse reflectance spectroscopy of PTTT and PTTB, Inset (upper right): the corresponding Tauc plots of the photocatalyst.

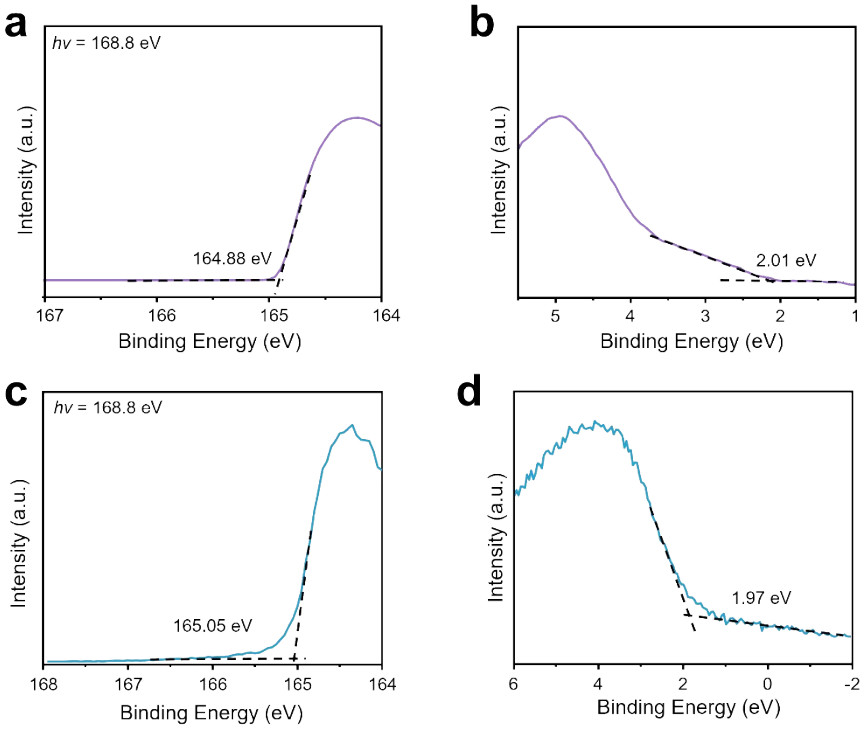

Fig. S8. Secondary electron cut-off of (a) PTTT and (c) PTTB measured by SRPES. Valence band spectra of (b) PTTT and (d) PTTB measured by SRPES.

As shown in Figs. S8a and S8c, the work functions (Φ) of PTTT and PTTB were calculated to be 3.92 and 3.75 eV, respectively, based on the secondary electron cut-off measurement. The valence band spectrum reveals that the highest occupied molecular orbital (HOMO) positions of PTTT and PTTB are located 2.01 eV and 1.97 eV below the Fermi level (Figs. S8b and S8d). Therefore, the HOMO levels of PTTT and PTTB relative to the vacuum level are -5.93 and -5.72 eV, respectively. Combining the optical bandgap derived from measurements (Fig. S7), the lowest unoccupied molecular orbital (LUMO) level of the PTTT and PTTB are -3.58 and -3.24 eV, respectively.

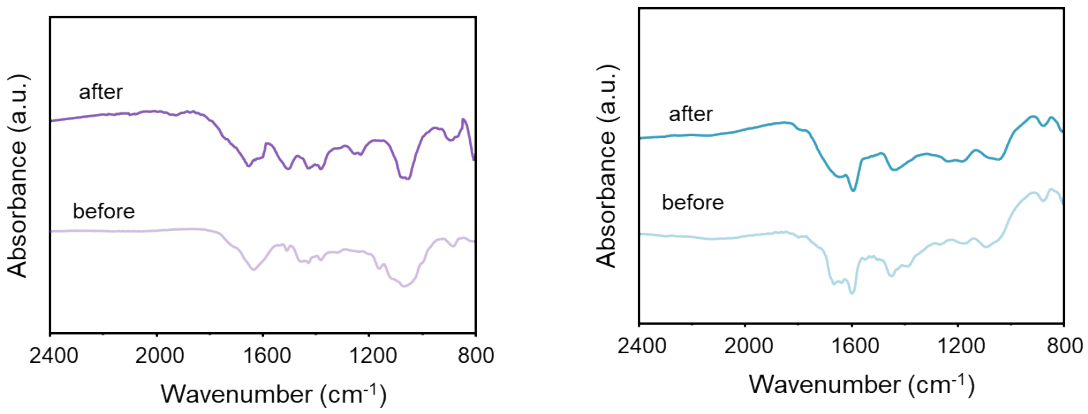

Fig. S9. FTIR of (a) PTTT and (b) PTTB before and after photocatalysis.

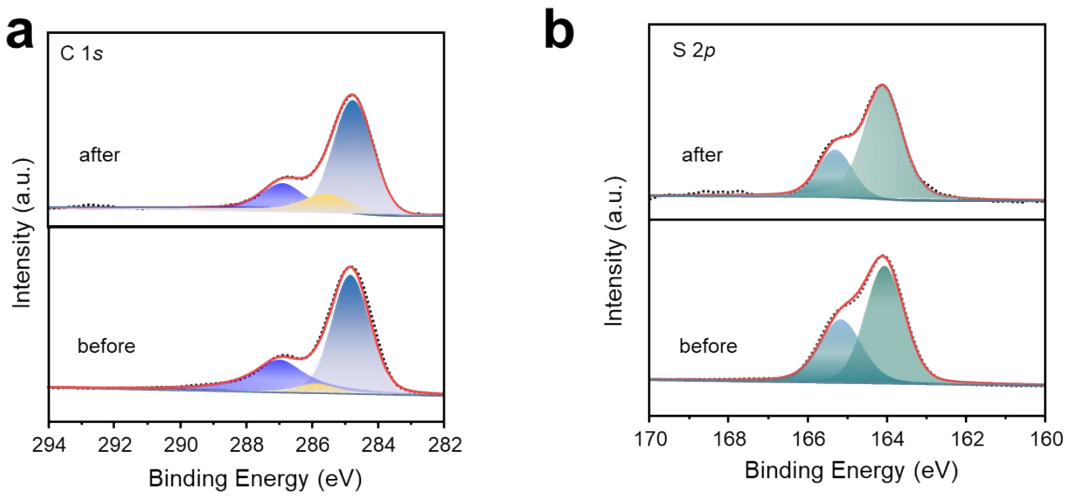

Fig. S10. High-resolution (a) C 1*s*, (b) S 2*p* of PTTT before and after photocatalysis.

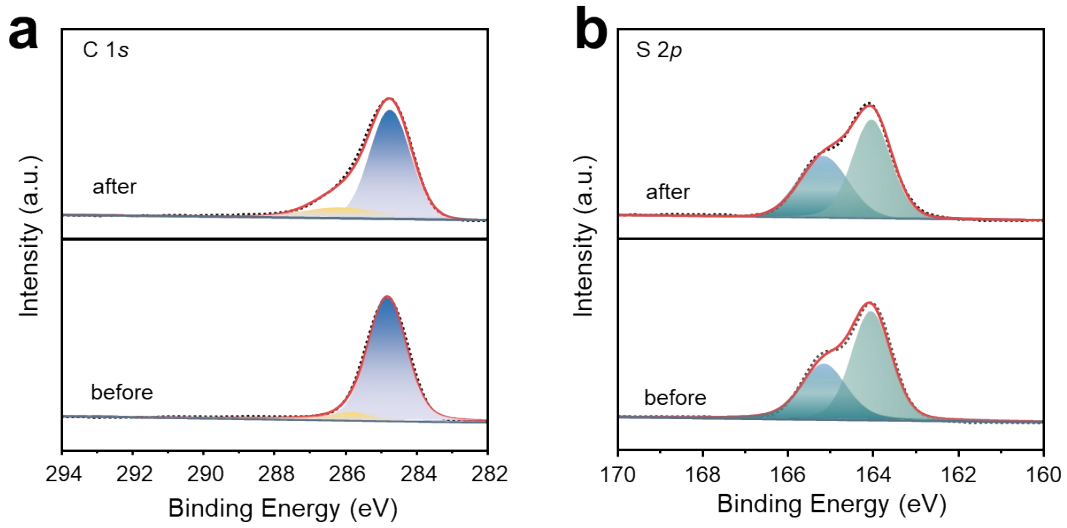

Fig. S11. High-resolution (a) C 1*s* and (b) S 2*p* of PTTB before and after photocatalysis.

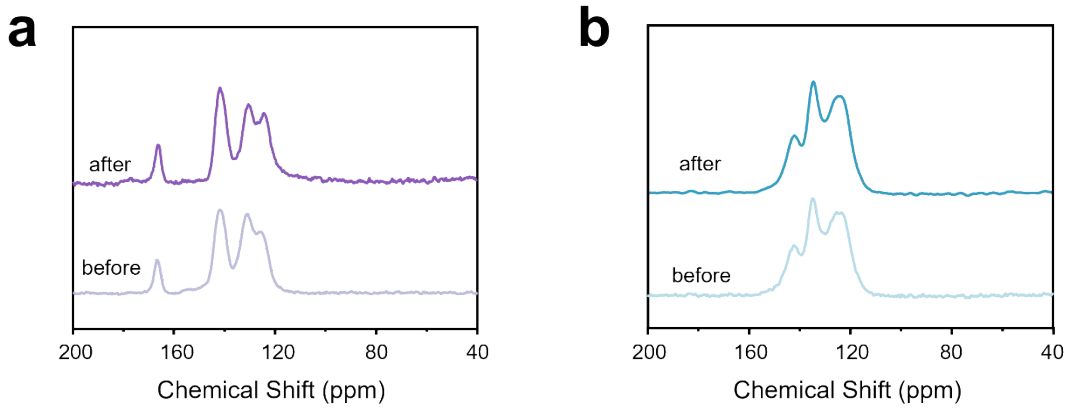

Fig. S12. Solid State ^{13}C CP/MAS NMR of (a) PTTT and (b) PTTB before and after photocatalysis.

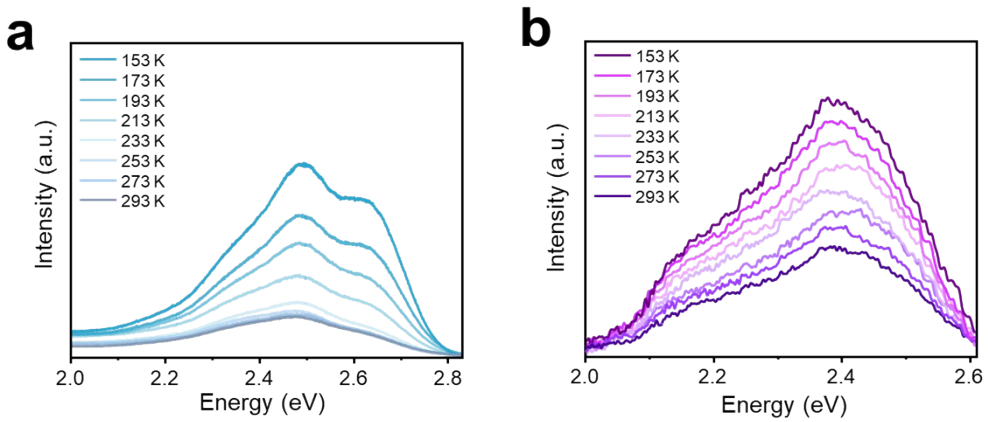

Fig. S13. Temperature-dependent PL spectra of (a) PTTB and (b) PTTT.

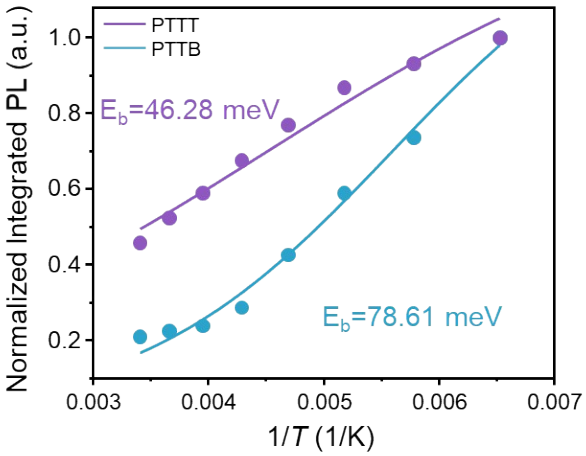

Fig. S14. Normalized integrated PL intensities of PTTB, and PTTT obtained from temperature-dependent PL measurements. The solid lines represent the exponential fitting of the data points.

The exciton binding energy (E_b) of PTTB, and PTTT were calculated via the following equation:

$$I(T) = \frac{I_0}{1 + Ae^{-\frac{E_b}{kT}}}$$

where I_0 is the intensity at 0 K, k is the Boltzmann constant, and T is the temperature during testing.

The thermal dissociation ratio (*T.D.R.*) were calculated via the following equation:

$$T.D.R. = e^{-\frac{E_b}{kT}}$$

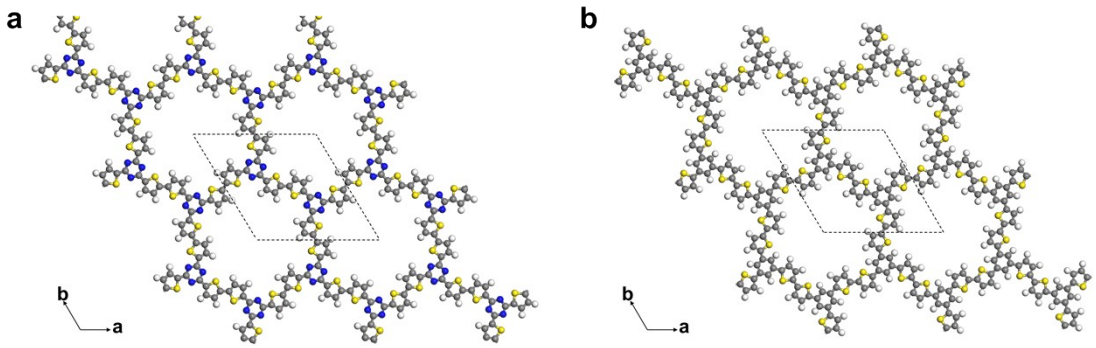

Fig. S15. Optimized structures of (a) PTTT and (b) PTTB. Gray, white, blue, and yellow spheres represent C, H, N, and S atoms, respectively. Lattice parameters for PTTT: a = b = 20.3 Å, α = β = 90°, γ = 120°. For PTTB: a = b = 20.9 Å, α = β = 90°, γ = 120°.

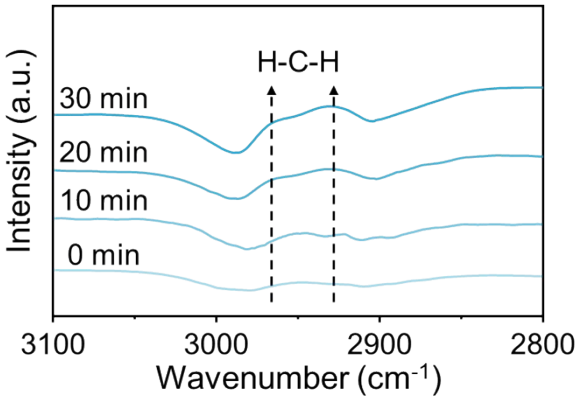

Fig. S16. *In situ* DRIFT spectra of PTTB recorded during photocatalytic H_2 evolution.

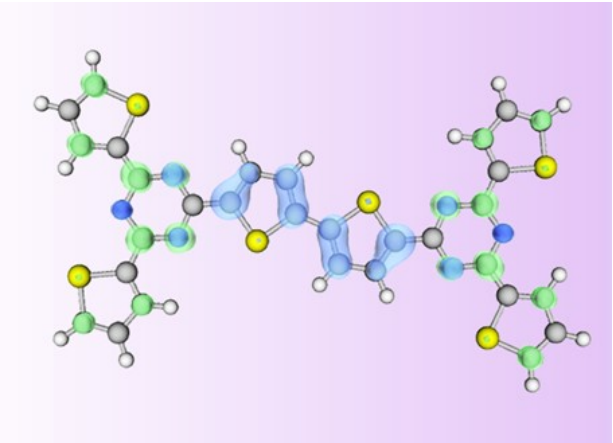

Fig. S17. Hole-electron analysis under excited states of PTTT. Excitation is predicted by TDDFT at the TD-PBE0/6-31G* level, with the green orbital representing the electron distribution and the blue orbital representing the hole distribution. Gray, white, blue, and yellow spheres represent C, H, N, and S atoms, respectively.

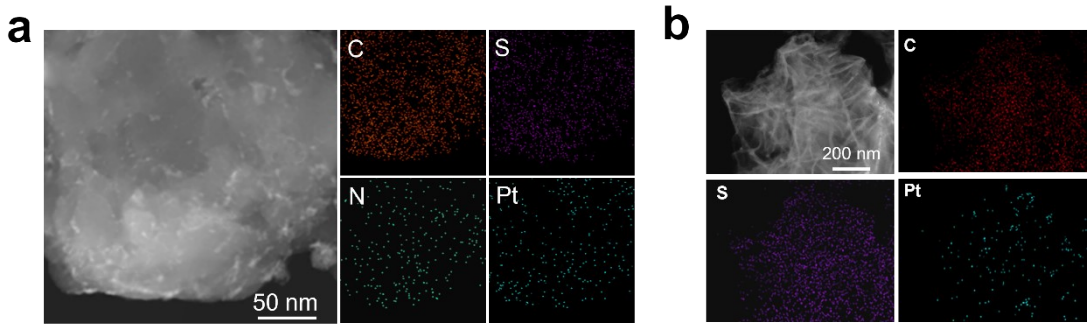

Fig. S18. High-resolution TEM images and the corresponding elemental mapping images of (a) Pt@PTTT and (b) Pt@PTTB.

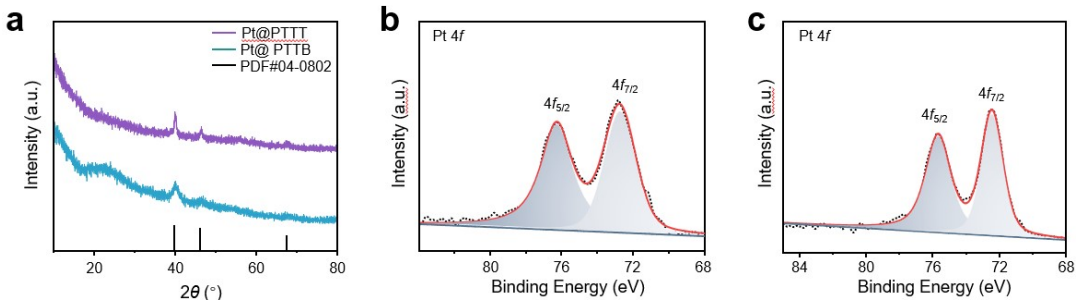

Fig. S19. PXRD patterns of Pt@PTTT and Pt@PTTB. The diffraction peaks at 39.8°, 46.2°, 67.5° can be indexed to the Pt (PDF#04–0802). High-resolution Pt 4*f* XPS spectra of (b) Pt@PTTT and (c) Pt@PTTB.

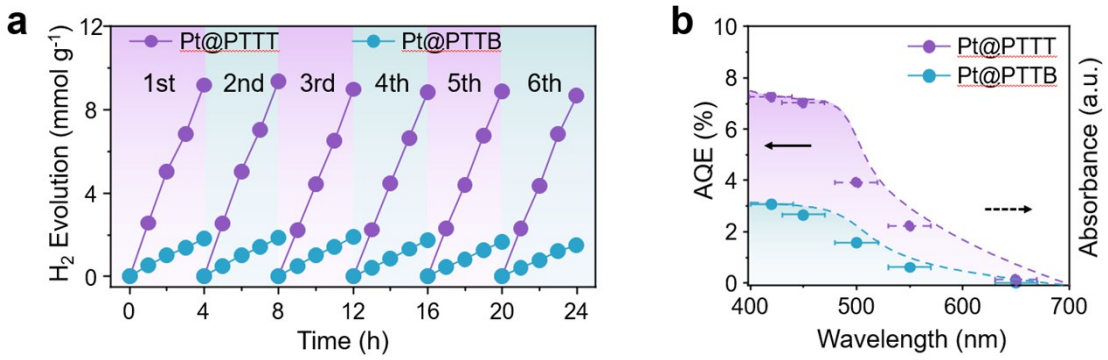

Fig. S20. (a) Typical time course of H_2 production under visible-light irradiation (λ > 420 nm) using Pt@PTTT and Pt@PTTB. (b) Wavelength-dependent AQE of photocatalytic water splitting by Pt@PTTT and Pt@PTTB.

Table S1. Comparison of HER performance of polymer photocatalysts under visible light irradiation without metal co-catalysts.

Photocatalysts	HER rate (mmol h^{-1} g^{-1})	Condition	Referencs
B-doped g-C_3N_4 (BCN-N)	0.17	λ = 420 nm (TEOA)	*Int. J. Hydrogen Energy* **2024**, *92*, 907.
Linear conjugated polymers (LF1)	0.04	λ > 420 nm (TEA)	*Chem. Commun.* **2022**, *58*, 10639.
LF2	0.53	λ > 420 nm (TEA)	
LF3	0.30	λ > 420 nm (TEA)	
PEB−DBT	0.10	λ > 420 nm (TEOA)	*Macromolecules* **2022**, *55*, 541.
PEB−DBT−xPY	0.54	λ > 420 nm (TEOA)	
P0	0.68	λ > 420 nm (TEA)	*J. Mater. Chem. A* **2021**, *9*, 8782.
P1	0.24	λ > 420 nm (TEA)	
phenylene co-polymers (P2)	0.13	λ > 420 nm (TEA)	*J. Mater. Chem. A* **2021**, *9*, 19958.
P36	0.19	λ > 420 nm (TEA)	
P37	0.017	λ > 420 nm (TEA)	
p-CzPh	0.13	λ > 420 nm (MeOH+TEA)	*J. Mater. Chem. A*, **2020**, *8*, 8700.
Cz-CMP3	0.16	λ > 420 nm (MeOH+TEA)	
PS-8	0.025	λ > 420 nm (TEOA)	*J. Mater. Chem. A* **2020**, *8*, 20062.
BP/CN	0.42	λ > 420 nm (MeOH)	*Adv. Mater.* **2018**, *30*, 1800128.
PTTB	0.11	λ > 420 nm (TEA)	*This work*
PTTT	0.45	λ > 420 nm (TEA)	

Reference

[1] G. Kresse, J. Furthmüller.*Phys. Rev. B* **1996**, 54, 11169.

[2] J. P. Perdew, K. Burke, M. Ernzerhof. *Phys. Rev. Lett*. **1996**, 77, 3865.

[3] J. K. Nørskov, J. Rossmeisl, A. Logadottir, L. Lindqvist, J. R. Kitchin, T. Bligaard, H.Jónsson. *J. Phys. Chem. B*. **2004**, 108, 17886.

[4] Tian Lu. *J. Chem. Phys*. **2024**, 161, 082503.

[5] J. K. Nørskov, T. Bligaard, A. Logadottir, J. R. Kitchin, J. G. Chen, S. Pandelov, U. Stimming. *J. Electrochem. Soc*. **2005**, 152, J23.